Wet scavenging process of particulate matter (PM_{10}): A multivariate complex network approach

Thomas Plocoste[a,b,*], Rafael Carmona-Cabezas[c], Eduardo Gutiérrez de Ravé[c], Francisco José Jiménez-Hornero[c]

[a] *Department of Research in Geoscience, KaruSphère SASU, Abymes 97139, Guadeloupe (F.W.I.), France*
[b] *Univ Antilles, LaRGE Laboratoire de Recherche en Géosciences et Energies (EA 4539), F-97100 Pointe-à-Pitre, France*
[c] *Complex Geometry, Patterns and Scaling in Natural and Human Phenomena (GEPENA) Research Group, University of Cordoba, Gregor Mendel Building (3rd floor), Campus Rabanales, 14071, Cordoba, Spain*

Abstract

This paper reports the results of research on PM_{10} wet scavenging by rainfall using a new multilayer complex networks called Multiplex Visibility Graphs (MVG). To the best of our knowledge, this work is the first to assess PM_{10} wet deposition using multivariate time series according to African dust seasonality. We considered 11 years of daily PM_{10} and rainfall data from the Guadeloupe archipelago. To analyse the impact of rainfall on PM_{10} behaviour, two MVG parameters were computed: the average edge overlap (ω) and the interlayer mutual information ($I_{PM_{10}Rainfall}$). On the 1-d scale, the ω results showed that the wet scavenging process was higher during the second half of the year when the high dust season and the rainy season are juxtaposed. This highlights a greater correlation between the microscopic structure of the signal, and the impact of rainfall on PM_{10} concentrations is more significant when the atmosphere is loaded with dust. The joint probability computed between the PM_{10} and rainfall nodes confirmed this trend. The $I_{PM_{10}Rainfall}$ results indicated a correlation between PM_{10} and

*Corresponding author

Email addresses: thomas.plocoste@karusphere.com (Thomas Plocoste), f12carcr@uco.es (Rafael Carmona-Cabezas), eduardo@uco.es (Eduardo Gutiérrez de Ravé), fjhornero@uco.es (Francisco José Jiménez-Hornero)

rainfall structures throughout the year. Furthermore, $I_{PM_{10}Rainfall}$ values were higher during the transition periods between winter and summer (and vice versa). Our study showed that MVG is a powerful technique for investigating the relationship between at least two nonlinear time series using a multivariate time series.

Keywords: PM_{10}, Wet scavenging, Multiplex visibility graphs, Complex networks, Caribbean area

1. Introduction

In geoscience, precipitation is a key component of the water cycle (Schneider et al., 2014) and of atmospheric circulation (Kidd and Huffman, 2011). In recent decades, the removal of atmospheric Particulate Matter (PM) by falling precipitation has greatly interested the scientific community (González and Aristizábal, 2012; Ouyang et al., 2015; Wu et al., 2018). This phenomenon, which can occur through liquid (rain) and solid (snow) forms of precipitation, is called "wet deposition" (Kim et al., 2012; Singh et al., 2016). Numerous studies have shown that wet scavenging of PM by rainfall is one of the primary precipitation processes for wet deposition (Laouali et al., 2012; Tiwari et al., 2012; Yoo et al., 2014; Singh et al., 2016; Olszowski, 2017; Wu et al., 2018; McClintock et al., 2019). Raindrops falling through the air column, bump into and collect air particles. Raindrops approach the particles, apply a force via the air as a medium, and change trajectory (Sonwani and Kulshrestha, 2019). The collision between the raindrops and the PM is conditioned by size and relative location (Olszowski, 2017). The two primary wet scavenging mechanisms related to rainfall are rainout (in-cloud scavenging) and washout (below-cloud scavenging) (Dallarosa et al., 2005; Tombette et al., 2009; Sonwani and Kulshrestha, 2019). Studies have shown that wet scavenging can remove 30% of the aerosols from the troposphere (Murakami et al., 1983; Schumann, 1989).

Over the past decades, two types of PM have received special attention due to their health impact: fine particles (particulate diameter < 2.5 μm, $PM_{2.5}$) and coarse particles (particles with diameters between 2.5 and 10 μm, $PM_{10-2.5}$) (Bayraktar et al., 2010; Plocoste and Calif, 2019). Epidemiological studies reveal that short- and long-term exposure to high concentrations of $PM_{2.5}$ and PM_{10} can cause human health problems (Weinmayr et al., 2010; Atkinson et al., 2014; Lu et al., 2015). The authors focused on PM_{10}, which also strongly impacts climate (Plocoste and Pavón-Domínguez, 2020b; Plocoste et al., 2020a).

In the Caribbean, air quality is frequently degraded by African dust (Euphrasie-Clotilde et al., 2020). Dust haze episodes primarily occur during summer (Petit et al., 2005; Prospero et al., 2014). Many studies present the processes that allow the transport of dust over the Atlantic Ocean (Perry et al., 1997; Prospero, 1999; Prospero and Lamb, 2003; Engelstaedter et al., 2006; Kumar et al., 2014; Euphrasie-Clotilde et al., 2020). As the wet scavenging of PM_{10} is a standard indicator of air quality in a given area, the aim of this study was to investigate the wet scavenging process of PM_{10} by rainfall in the Caribbean Basin. Additionally, we aim to determine whether there is a link between wet scavenging efficiency and African dust seasonality.

A newly developed method termed Multiplex Visibility Graph (MVG) was used to perform this study (Lacasa et al., 2015). The methodology is based on a previous technique called Visibility Graph (VG), first introduced by Lacasa et al. (2008). The main idea is to transform a time series into a complex network, which can later be analysed, and to preserve some of the original information. Most of the variants of this method focus on analysis of a single time series (Luque et al., 2009; Lan et al., 2015; Carmona-Cabezas et al., 2019b; Iacovacci and Lacasa, 2019) and have been applied to applications related to univariate time series (Mali et al., 2018; Carmona-Cabezas et al., 2019a; Plocoste et al., 2021b). However, owing to their stochastic properties, atmospheric processes are frequently related to numerous degrees of freedom; that is, their behaviour is governed by a multivariate time series. To overcome this drawback, the MVG technique applies the visibility approach to examine nonlinear multivariate time series (Lacasa et al., 2015). After transforming the time series into complex networks, the results were used to build a multi-layered structure that could be analysed. Owing to recent advances in the theory of multilayer networks (Bianconi, 2013; Kivelä et al., 2014; Battiston et al., 2014; Lacasa et al., 2015), additional information can be retrieved from the original multivariate time series. To the best of our knowledge, no study has yet investigated PM_{10} wet scavenging using a multivariate time series. Here, 11 years of daily PM_{10} and rainfall data from the Guadeloupe archipelago were analysed.

2. Site and data collection

The Guadeloupe archipelago (16.25°N −61.58°W) is a French overseas region located in the central Caribbean Basin (Plocoste et al., 2019). The small territory (∼1,800 km^2; 390,250 inhabitants) has an insular tropical climate with meteorological characteristics that vary by location due to microclimates (Bertin and Frangi, 2013). According to the Köppen-Geiger climate classification (Peel et al., 2007), Guadeloupe is in the "Af (tropical rainforest)" category.

For this study, time series of Particulate Matter (PM_{10}) and rainfall were used. Hourly PM_{10} data were provided by Gwad'Air Agency (http://www.gwadair.fr/), which manages the Guadeloupe air quality network. PM_{10} concentrations were measured using the Thermo Scientific Tapered Element Oscillating Microbalance (TEOM) models 1400ab and 1400-FDMS. From 2005 to 2017, the air quality network-principally located at the centre of the island-has only one PM_{10} sensor at Pointe-à-Pitre (16.2422°N 61.5414°W) from 2005 to 2012 and at Baie-Mahault (16.2561°N 61.5903°W) since 2015. Because of the proximity between the air quality stations ($\sim$5.5 km), PM_{10} measurements were performed under the same environmental conditions. Rainfall measurements were made by Météo France at the international airport of Pôle Caraïbes at Abymes (16.2630°N 61.5147°W) using a Precis-Mecanique 3070. As with the PM_{10} time series, the Météo France observations are an hourly rainfall time series. Both measurements were made in the insular continental regime (Plocoste et al., 2018; Plocoste and Pavón-Domínguez, 2020a). To assess the possible wet scavenging phenomenon over an entire day, hourly PM_{10} data were converted into daily average values, whereas rainfall data were converted into daily average and daily sum values. By computing the Pearson correlation coefficient between the daily average PM_{10} and the daily rainfall data (sum then average), the same result was obtained (R= -0.14). Many studies demonstrate the cumulative effect of rainfall on atmospheric processes (Winstanley, 1973; Johnson and Ciesielski, 2000). In addition, to account for hours with and without rainfall (0 mm) in a day, the authors favoured the sum over the average for the stochastic analysis. Thus, 11 years of simultaneous measurements between the daily average PM_{10} and the daily sum of rainfall were available for this study (a total of 3,849 points per time series). Figure 1 shows the sequence of the analysed time series. A slight lag appears to exist between the groups of peaks.

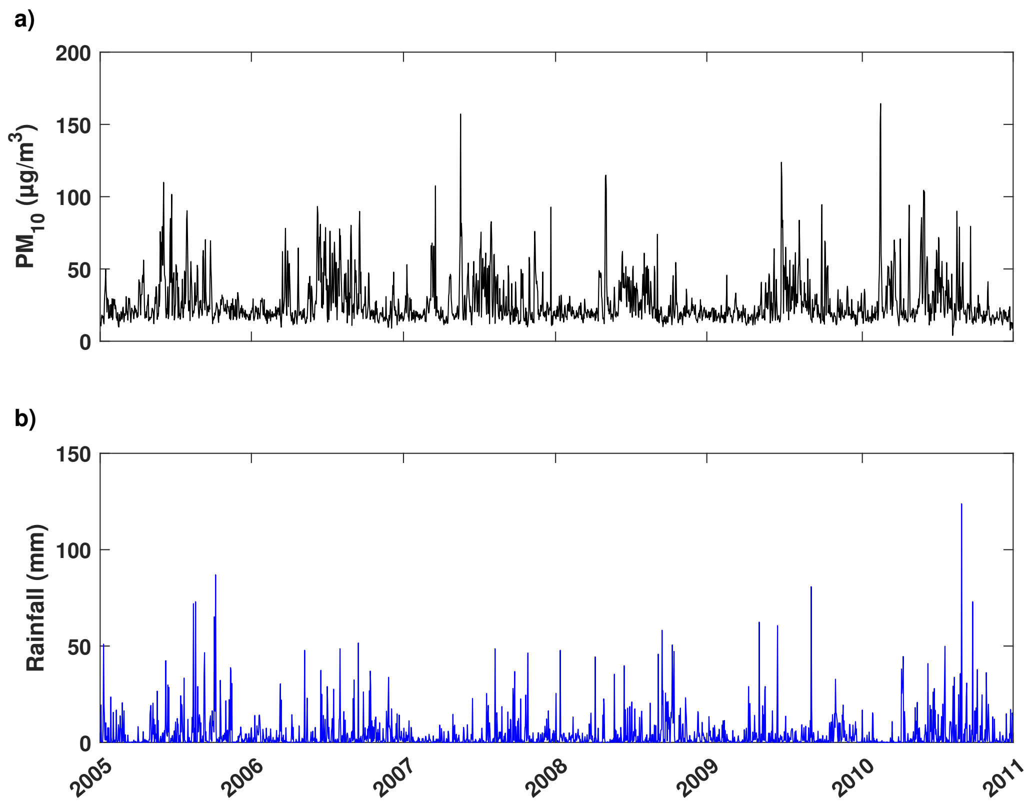

Figure 1: Illustration of simultaneous measurement sequences between (a) daily average PM_{10} concentrations and (b) the daily sum of rainfall between 2005 and 2011.

3. Theoretical framework

3.1. Visibility graphs

A graph is a mathematical object composed of a set of vertices (or nodes) which are connected by a set of lines or edges. A relatively recent tool called Visibility Graph (VG) allows the transformation of two-dimensional sets of points into graphs or networks (Lacasa et al., 2008). VG has great applicability for time series analysis and produces networks that inherit many of the properties of the original time series (Lacasa and Toral, 2010).

The points in the time series correspond to the nodes in the graph. The edges of the graph (which connect nodes) are selected by checking which pairs of points meet the visibility criterion, which is as follows: two points from the time series (t_a, y_a) and (t_b, y_b) are connected only if any other point (t_c, y_c) located between them $(t_a < t_c < t_b)$ fulfils the following relationship (Lacasa et al., 2008):

$$y_c < y_a + (y_b - y_a)\frac{t_c - t_a}{t_b - t_a} \tag{1}$$

To construct the graph, this algorithm was applied to every pair of points in the signal. Two consecutive nodes are always connected, because there are no intermediate points.

A graph is commonly expressed via its adjacency matrix, whose rows store the information of each node. If an element a_{ij} is equal to 1, nodes i and j are connected, the opposite is true if a_{ij} is equal to 0. In the case of a time series with N points, the resulting VG is represented by an N×N adjacency matrix, which has special properties that facilitate computation; the adjacency matrix is symmetric ($a_{ij} = a_{ji}$) and hollow ($a_{ii} = 0$); additionally, all the nearest neighbours are visible to one other ($a_{ij} = 1$ for $j = i \pm 1$). In general, the adjacency matrix has the following form (Carmona-Cabezas et al., 2019a):

$$V = \begin{pmatrix} 0 & 1 & \cdots & a_{1,N} \\ 1 & 0 & 1 & \vdots \\ \vdots & 1 & \ddots & 1 \\ a_{N,1} & \cdots & 1 & 0 \end{pmatrix} \tag{2}$$

3.2. Degree centrality

Degree is the most commonly used of the principal properties that can be studied from a graph and one of the centrality parameters used to measure the importance of different nodes in the graph with relation to the rest of them, using different criteria (Latora et al., 2017). The degree of a node (k_i) measures (in an undirected graph) the number of nodes that are reciprocally connected to a given node. By considering the adjacency matrix, the degree can be computed as $k_i = \sum_j a_{ij}$.

Once the degree of every point is computed, a degree probability distribution $P(k)$ can be obtained for the graph (here, VG). $P(k)$ accounts for the probability of having each value of degree in the graph. To obtain information on the nature of the series, the degree distribution is analysed (Lacasa et al., 2008; Mali et al., 2018; Pierini et al., 2012). If the right tail of the degree distribution (for high values of degree) can be fitted by a power law such as $P(k) \propto k^{-\gamma}$, the time series has a fractal nature (Lacasa et al., 2008). This part of the distribution is related to the hubs (nodes with the highest degrees), which are, by definition, rare in a graph. The exponent in the power law is the coefficient, which is related to the Hurst exponent in series related to Brownian motion (Lacasa et al., 2009).

3.3. Multiplex visibility graph

Another application of VGs in the context of multivariate analysis, is the use of multi-layered networks. This methodology was recently introduced as *Multiplex Visibility Graph (MVG)* (Lacasa et al., 2015). The main idea behind MVG is to build each of the layers M with VGs from the different variables of the study. Therefore, as VG is represented by its adjacency matrix, so MVG is identified by a vector of adjacency matrices $\Omega = \{A^{[1]}, A^{[2]}, ..., A^{[M]}\}$. In the last expression, $A^{[\alpha]}$ corresponds to the VG adjacency matrix of the VG in the α-dimension (or layer in the multiplex), which comes from the α variable of the multivariate time series (see Figure 2, where PM_{10} and rainfall sample time series are transformed for illustrative purposes).

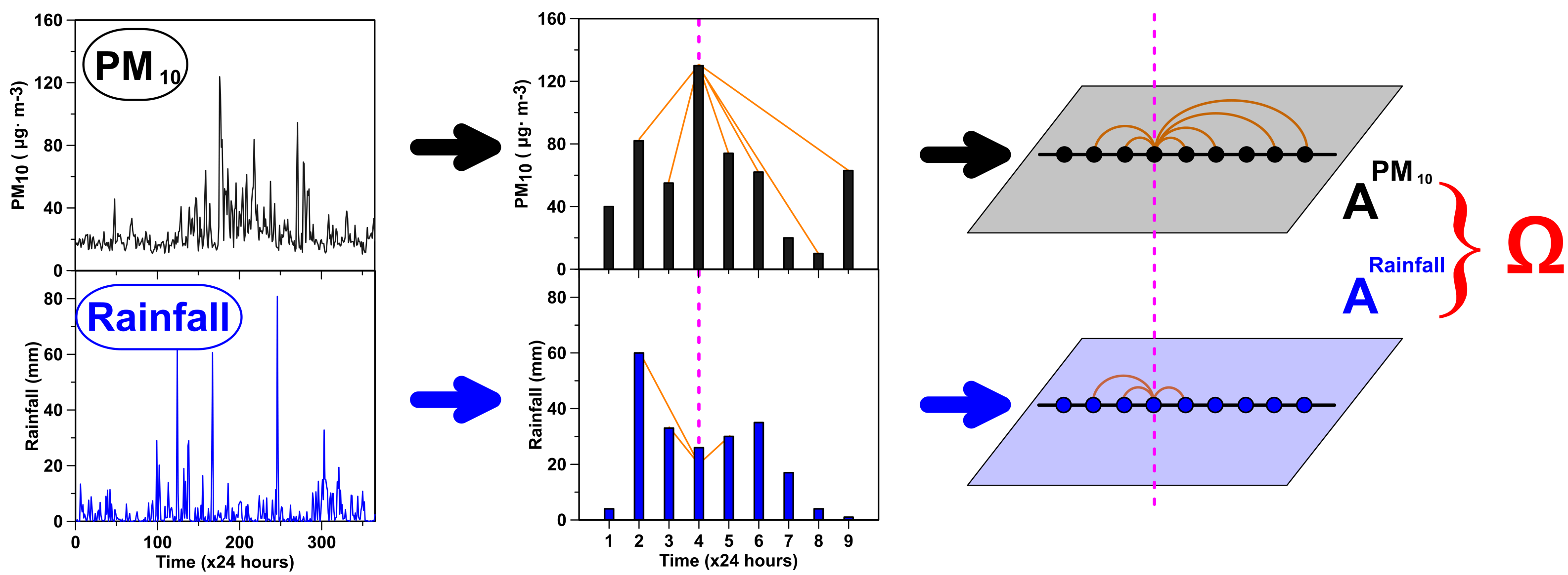

Figure 2: PM_{10} and rainfall time series (left) are converted into complex networks with the VG algorithm (centre), which is described by an adjacency matrix ($A^{PM_{10}}$ and $A^{Rainfall)}$). Then, both are combined to design a two-layered MVG, called Ω (right image).

After construction, MVG is analysed to obtain information regarding the system of the time series. The two measures used for such purposes (Nicosia and Latora, 2015) and chosen for this work are *Average Edge Overlap* (ω) and *Interlayer Mutual Information* ($I_{\alpha,\beta}$). ω averages the number of layers on which a given edge between a pair of nodes can be found. $I_{\alpha,\beta}$ measure the correlations between the degree distributions of the given layers α and β. In this study, the layers correspond to daily PM_{10} concentrations and total rainfall.

The computation is relatively straightforward after the MVG and degree distributions of each layer are obtained. Equation 3 shows the formula to compute the ω of a given MVG (Lacasa et al., 2015):

$$\omega = \frac{\sum_i \sum_{j>i} \sum_\alpha a_{ij}^{[\alpha]}}{M \sum_i \sum_{j>i} \left(1 - \delta_{0,\sum_\alpha a_{ij}^{[\alpha]}}\right)} \tag{3}$$

All quantities were previously defined in the text; $\delta_{0,\sum_\alpha a_{ij}^{[\alpha]}}$ corresponds to a Kronecker delta, which is 1 when $\sum_\alpha a_{ij}^{[\alpha]}$ is null, and otherwise 0. The maximum value of $\omega = 1$ indicates that all the layers and, therefore, the time series are identical. Conversely, the minimum possible value of $\omega = 1/M$ indicates that every edge in the MVG can be found only in a singular layer. Overall, this quantity provides an idea of the expected number of layers on which an edge can be found. In addition, a high ω value indicates a high correlation in the microscopic structure of the signal (Lacasa et al., 2015).

Additionally, $I_{\alpha,\beta}$ is defined in Equation 4 (Lacasa et al., 2015):

$$I_{\alpha,\beta} = \sum_{k^{[\alpha]}} \sum_{k^{[\beta]}} P(k^{[\alpha]}, k^{[\beta]}) log \frac{P(k^{[\alpha]}, k^{[\beta]})}{P(k^{[\alpha]}) P(k^{[\beta]})} \tag{4}$$

where $P(k^{[\alpha]}, k^{[\beta]})$ is the joint probability of having a degree of $k^{[\alpha]}$ in layers α and $k^{[\beta]}$ in layer β that can be obtained using the following formula:

$$P(k^{[\alpha]}, k^{[\beta]}) = \frac{N_{k^{[\alpha]},k^{[\beta]}}}{N} \tag{5}$$

where $N_{k^{[\alpha]},k^{[\beta]}}$ is the number of nodes with a degree of $k^{[\alpha]}$ in layer α and $k^{[\beta]}$ in layer β; $N_{k^{[\alpha]},k^{[\beta]}}$ is divided by N, which is the total number of nodes or points in the time series.

4. Results and Discussion

4.1. Preliminary analysis

We conducted a preliminary analysis to investigate PM_{10} and rainfall seasonality throughout the year. Figure 3 illustrates the monthly average PM_{10} concentrations and the monthly summation of rainfall data over 11-y period. Seasonality is observed in both curves, with a high dust season from May to September (Plocoste and Pavón-Domínguez, 2020b) and a rainy season from July to November (Bertin and Frangi, 2013). Van der Does et al. (2020) observed the same behaviour for both parameters in Barbados. The Inter-Tropical Convergence Zone (ITCZ) dynamics throughout the year play a key role in these seasonal behaviours. In summer, the activation of dust sources from the Saharan and Sahelian deserts coupled with the upward northward movement of the ITCZ ($10-20°$N) (Moulin et al., 1997; Adams et al., 2012; Euphrasie-Clotilde et al., 2020) allows the transport of dust plumes from the African coast to the Caribbean area (Petit et al., 2005; Prospero et al., 2014; Euphrasie-Clotilde et al., 2021). According to a statistical study lasting over a decade (Plocoste et al., 2020b), average PM_{10} and kurtosis are 1.5 times higher and 5.5 times lower during the high dust season, respectively, due to the recurrence of dust plumes compared with the low dust season. From October to April, PM_{10} concentrations are primarily related to marine aerosols (Clergue et al., 2015; Rastelli et al., 2017), because of the insular context of the Guadeloupe archipelago. These aerosols are advected by trade winds which blow continuously from east to west across the Atlantic Ocean (Plocoste et al., 2014; Plocoste and Pavón-Domínguez, 2020a). Consequently, the contribution of marine aerosols to PM_{10} concentrations remains constant throughout the year. Figure 3 shows that the standard deviations exhibit their lowest values from October to April. Thus, marine aerosols are one of the primary constituents of the PM_{10} background atmosphere (Plocoste et al., 2021a). The ITCZ movement toward the north generates precipitation carried by trade winds during the boreal summer (the rainy season) (Giannini et al., 2000; Muñoz et al., 2008). During the boreal winter (mid-January to March), the ITCZ awakens the Azores anticyclone due to its southerly movement, which reduces cloud generation (the dry season) (Bertin and Frangi, 2013).

4.2. Degree distribution

4.2.1. Overall analysis

Before performing a profound analysis of the impact of rainfall on PM_{10} concentrations in the MVG frame, both time series were analysed separately in the VG frame. The classical first approach is to study the degree distribution $P(k)$ of each time series. Figure 4(a) and 4(b) show the degree distributions obtained for the PM_{10} and rainfall time series over the 11-y period, respectively. Both plots highlight the fractal nature of the time series. The tail region of $P(k)$ in the log-log plot can be fitted by a power law, such as $P(k) \propto k^{-\gamma}$, where $\gamma_{PM_{10}}$ and $\gamma_{rainfall}$ equal 3.11, and 2.84,

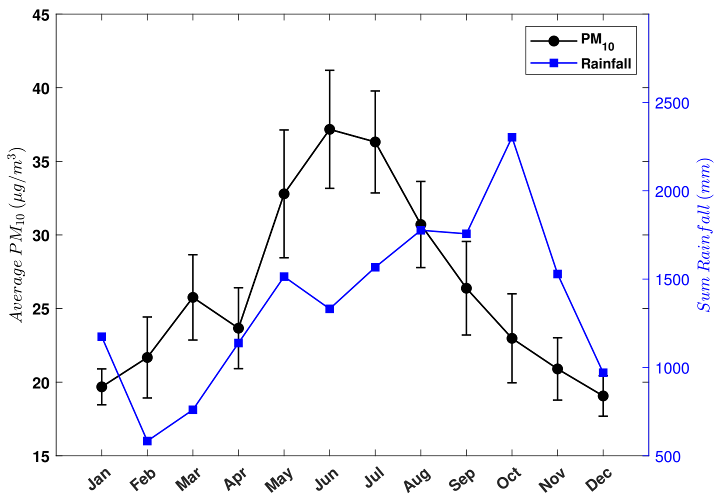

Figure 3: Monthly conditional average of PM_{10} and rainfall time series over the 11-y period; here, a representative year for one decade. The whiskers depict the standard deviations.

respectively. In the literature, the fractal nature of the PM_{10} (Dong et al., 2017; Nikolopoulos et al., 2019; Plocoste et al., 2021b) and rainfall (Olsson et al., 1993; Breslin and Belward, 1999; Maskey et al., 2016) data has been observed.

To assess the behaviour of the highest degree (so-called hubs), the time series values versus their degrees (v-k plot) were analysed for each parameter as introduced by Pierini et al. (2012). Figure 4(c) and 4(d) illustrate the v-k plot for the PM_{10} and rainfall data, respectively. In both cases, the hubs were related to the highest values of each time series. Carmona-Cabezas et al. (2019a) found the same tendency for hubs of a tropospheric ozone time series in Cadiz, Spain. The value of precipitation has an almost linear relationship to the degree of rainfall. Thus, the degree of the rainfall nodes can be used to identify both high and low rainfall values. In addition, the

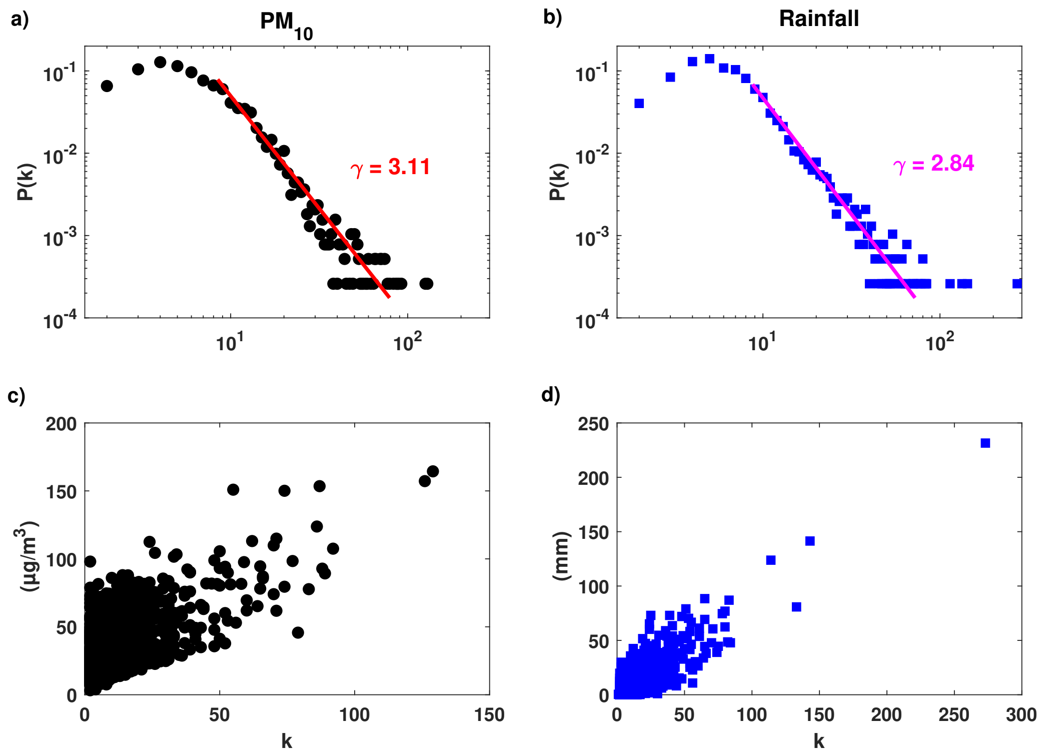

Figure 4: At the top, degree distribution of the visibility graph for (a) PM_{10} and (b) rainfall in a log-log plot for all the data. A the bottom, the relationship between the time series values and their degrees in (c) PM_{10} and (d) rainfall.

PM_{10} dot distribution appears more heterogeneous, because of the wide annual variability of African dust haze (Plocoste et al., 2017, 2020a).

4.2.2. Monthly analysis

We use the first centrality measure (degree centrality) to study the importance of the node for PM_{10} and rainfall throughout the year (Carmona-Cabezas et al., 2019a). Figure 5(a) and 5(b) highlight the monthly behaviour of the average degree and standard deviation from the degree distribution of the PM_{10} and rainfall time series. A trend merged in both curves. The decay of PM_{10} hubs begins at the onset of the high dust season (May-September) (Plocoste and Pavón-Domínguez, 2020b; Plocoste et al., 2021b); the decay for rainfall hubs begins at the onset of the hurricane season (June–October) (Tartaglione et al., 2003; Dunion, 2011) in the Caribbean Basin. Figure 3 shows that the monthly behaviour of PM_{10} and rainfall over the period of a decade confirms this trend, increases in PM_{10} and rainfall begin in May and June, respectively. The above-mentioned results show the impact of seasonality on node distribution and highlight that the VG frame is sensitive to time-series behaviour.

4.3. Multiplex visibility graph

After performing the analysis of the PM_{10} and rainfall univariate time series in the VG frame (i.e., transformation of the time series into a complex network), both complex networks were combined to design a two-layered multivariate network. Here, we investigate the wet scavenging process of PM_{10} by rainfall. The authors focused on two approaches, which demonstrate the abundance of single edges across layers (average edge overlap) and the presence of interlayer correlations of the node degrees (interlayer mutual information) (Lacasa et al., 2015; Nicosia and Latora, 2015). The first approach measures the overall coherence in the multivariate time series, and the second evaluates structural correlation.

4.3.1. Average edge overlap analysis

Figure 6 illustrates the monthly average edge overlap values (ω) and their standard deviations over the 11-y period. $\omega > 1/M$ and $\omega < 1$; thus, the two layers are different, and edges can be found in both layers. These

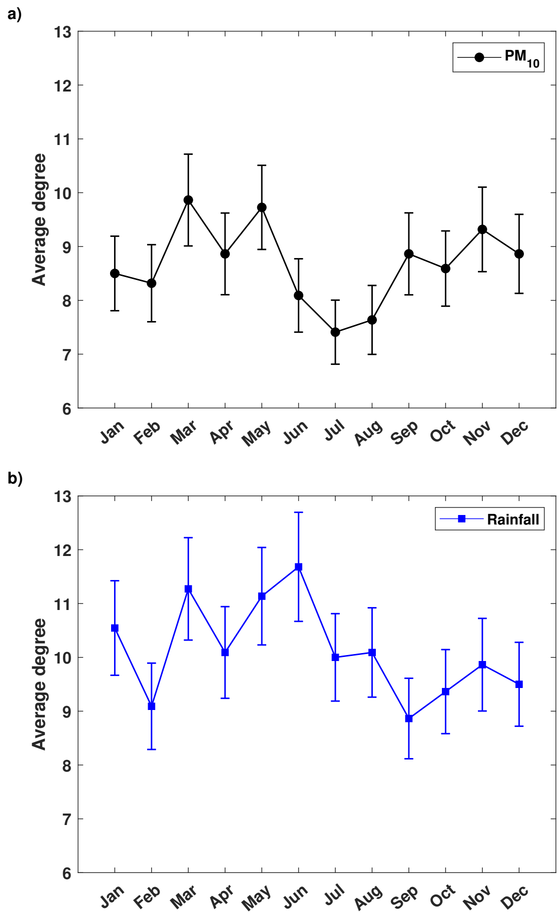

Figure 5: Computed average degree and standard deviation from the degree distribution of each month over the 11-y period for (a) PM_{10} and (b) rainfall. Each monthly value is the average of the computed 11-y values.

two criteria prove that there is an interaction between PM_{10} and rainfall in the MVG frame. ω is a sensitive parameter with small variations (increases and decreases) (Lacasa et al., 2015). Here, ω was almost constant from January to June. ω values are higher from July to December and peaked in September, indicating a greater correlation in the microscopic structure of the signal (Lacasa et al., 2015; Carmona-Cabezas et al., 2020) that represents interaction on the order of 1-d, which is the minimum time resolution. Therefore, at the 1-d scale, the wet scavenging process of PM_{10} by rainfall is more significant during the last six months of the year. A 20-y precipitation study in the Luquillo Mountains of Puerto Rico McClintock et al. (2019) also found a summer maximum in wet dust deposition. Physically, these findings make sense, as the summer corresponds to the high dust (Plocoste and Pavón-Domínguez, 2020b) and rainy (Bertin and Frangi, 2013) seasons in the Caribbean Basin. The atmosphere is loaded with dust, and the impact of rainfall on PM_{10} is greater. Tiwari et al. (2012) observed that low PM_{10} concentrations in New Delhi occurred during the monsoon (August-September) season due to the washout phenomenon. A 10-y study of air pollutants (PM_{10}, CO, NO_2, SO_2, and O_3) and precipitation over South Korea highlighted that PM_{10} is most effectively scavenged by summertime rainfall due to its particulate nature (Yoo et al., 2014). Because of data availability, determining which wet scavenging process (rainout or washout) is more efficient is difficult (Pillai et al., 2002; Tombette et al., 2009; Bayraktar et al., 2010). According to Sonwani and Kulshrestha (2019), the level of aerosols in and under clouds at the time of precipitation is crucial, as it determines whether both phenomena occur simultaneously.

During the high dust season, the wet scavenging phenomenon naturally reduces PM_{10} concentrations in the atmosphere. Due to the impact on respiratory and cardiovascular diseases, diminishing PM_{10} concentrations after dust outbreaks is crucial (Gurung et al., 2017; Zhang et al., 2017; Momtazan et al., 2019; Feng et al., 2019). African Easterly Waves (AEWs) (Prospero and Carlson, 1981; Plocoste et al., 2021a), which precede and follow the dust plumes, are the principal generator of precipitation during the high dust period (Dominguez et al., 2020) and regulate PM_{10} concentrations in the Caribbean area.

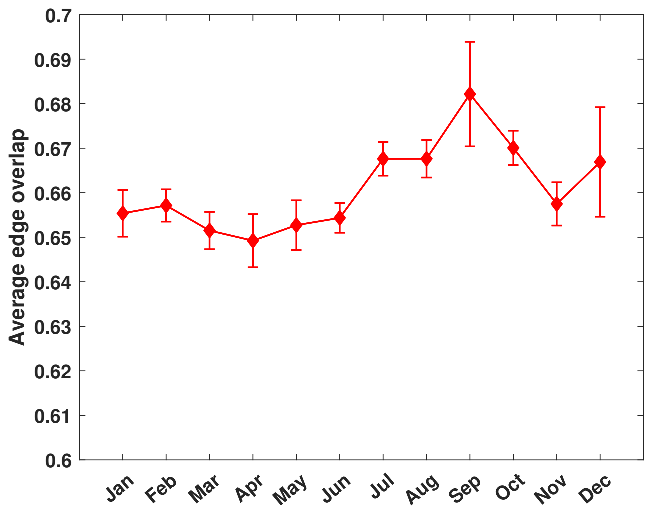

Figure 6: 11-y monthly average edge overlap values (ω) and their standard deviations.

4.3.2. Interlayer mutual information analysis

The relationship between PM_{10} concentrations and rainfall can also be determined by studying the node distribution in the MVG layers. Equation 4 shows that the joint probability between the PM_{10} and rainfall nodes ($P(k^{[PM_{10}]}, k^{[Rainfall]})$) is a building block of the interlayer mutual information ($I_{PM_{10},Rainfall}$). Thus, we first computed the joint probability before performing the interlayer mutual information analysis.

Figure 7(a) and 7(b) illustrate the quantity $P(k^{[PM_{10}]}, k^{[Rainfall]})$ for the low dust season (October to April) and the high dust season (May to September) for the 11-y period. In these Figures, the colours indicate the probability that a node in the MVG has a degree equal to $k^{PM_{10}}$ and $k^{Rainfall}$ in the layers corresponding to PM_{10} and rainfall VG, respectively. Overall, the most likely combinations of k values were those below a value of 20. For higher degrees ($k > 60$), $P(k^{[PM_{10}]}, k^{[Rainfall]})$ becomes less significant. The probability asymptotically approaches both the X and Y axes. According to Carmona-Cabezas et al. (2020), as the degree increases, the probability of finding $k^{PM_{10}}$ and $k^{Rainfall}$ with close values decreases exponentially. This demonstrates alternation between the hubs of the two time series. Due to the wet scavenging phenomenon, high daily values of PM_{10} and rainfall are less likely to occur on the same day. Figure 7(a-b) shows a difference in behaviour between both seasons. A concentration of probability is more pronounced in the high dust season (Figure 7(b)), and higher values in a low-degree area add red to the plot. In addition, the overall shape of the plot shrinks for the same period and has shorter tails. These results are consistent with those obtained for ω. The impact of rainfall on PM_{10} concentrations in the atmosphere more loaded with dust from May to September is more efficient because of a more significant wet scavenging phenomenon (Tiwari et al., 2012; Yoo et al., 2014).

Figure 7(c) shows the monthly $I_{PM_{10},Rainfall}$ computed over the 11-y period. The interlayer mutual information, which provides an idea of the typical amount of information flow in the system (Lacasa et al., 2015), is directly related to the joint probability and also measures the correlation between degrees in the system. Thus, the interlayer mutual information may indicate the degree of correlation among the distributions and, hence, the behaviour of the two series. Because $I_{PM_{10},Rainfall} > 1$, $k^{PM_{10}}$ and $k^{Rainfall}$ always have higher correlations in May ($I_{PM_{10},Rainfall} = 1.25$), August ($I_{PM_{10},Rainfall} = 1.14$) and November ($I_{PM_{10},Rainfall} = 1.15$). A study in the Caribbean basin by Gouirand et al. (2020) showed that the averages transition dates from winter to summer and from summer to winter occurred on average 13 May ($\pm$ 9 days) and 26 October ($\pm$ 12 days), respectively.

These transition periods correspond to comparatively high $I_{PM_{10},Rainfall}$ values. Due to the standard deviations, the winter to summer transition always occurs in May, whereas the summer to winter transition can occur in October or November. This could explain why the May peak was much larger. In addition, May corresponds to the beginning of the high dust season (Plocoste and Pavón-Domínguez, 2020b), whereas November corresponds to the end of the rainy season (Bertin and Frangi, 2013). Therefore, these periods feature strong inter-layer correlations between $k^{PM_{10}}$ and $k^{Rainfall}$.

5. Conclusion

In conclusion, our results clearly highlight the efficiency of multilayer complex networks for tracking the correlations between particulate matter (PM_{10}) and rainfall time series. The aim of this study was to investigate the wet scavenging phenomenon of PM_{10} by rainfall in the Caribbean area using MVGs. We highlighted the fractal nature of both time series and found that the highest degrees (hubs) are related to the highest values in the VG frame. The relationship between the values and degrees of PM_{10} is less homogeneous than that of rainfall due to annual intermittency. The monthly degree centrality analysis indicated the seasonality of both time series. On the 1-d scale, the average edge overlap (ω) monthly analysis highlighted the wet scavenging process of PM_{10} by rainfall throughout the year. However, this process seems to be more significant during the last six months of the year, when the high dust and rainy seasons are juxtaposed. The joint probability results between the PM_{10} and rainfall nodes according to African dust seasonality confirmed the trend observed from the ω values. The atmosphere is loaded with dust during the high dust season, and rainfall helps restore the

PM_{10} atmospheric balance. Thus, the overall coherence in the multivariate time series was higher from July to December. The interlayer mutual information ($I_{PM_{10}Rainfall}$) monthly analysis showed a correlation between PM_{10} and rainfall structures throughout the year. $I_{PM_{10}Rainfall}$ values were higher during the transition periods between winter and summer (and vice versa) in the Caribbean Basin. We assume that the transition periods allow the homogenisation of the multivariate time series before the usual trend is resumed. To better quantify the impact of the wet scavenging process on PM_{10}, a future analysis of rainwater chemistry (organic and elemental carbon) related to rainfall intensity will be conducted.

Acknowledgements

The authors are very grateful to the anonymous reviewers for their valuable comments and constructive suggestions, which helped us to improve the quality of the paper substantially. The authors would like to thank Guadeloupe air quality network (Gwad'Air) and the French Weather Office (Météo France Guadeloupe) for providing air quality and meteorological data. A special thanks to Mr. France-Nor Brute (Data Scientist) for data assistance. Group TEP-957 authors gratefully acknowledge support of the Research Program of the University of Cordoba (2021), Spain.

Disclosure statement

No potential conflict of interest was reported by the authors.

Funding

The authors declare that they have not received any fund for the present paper. The paper is the sole work of the authors and is not a part/product of any project.

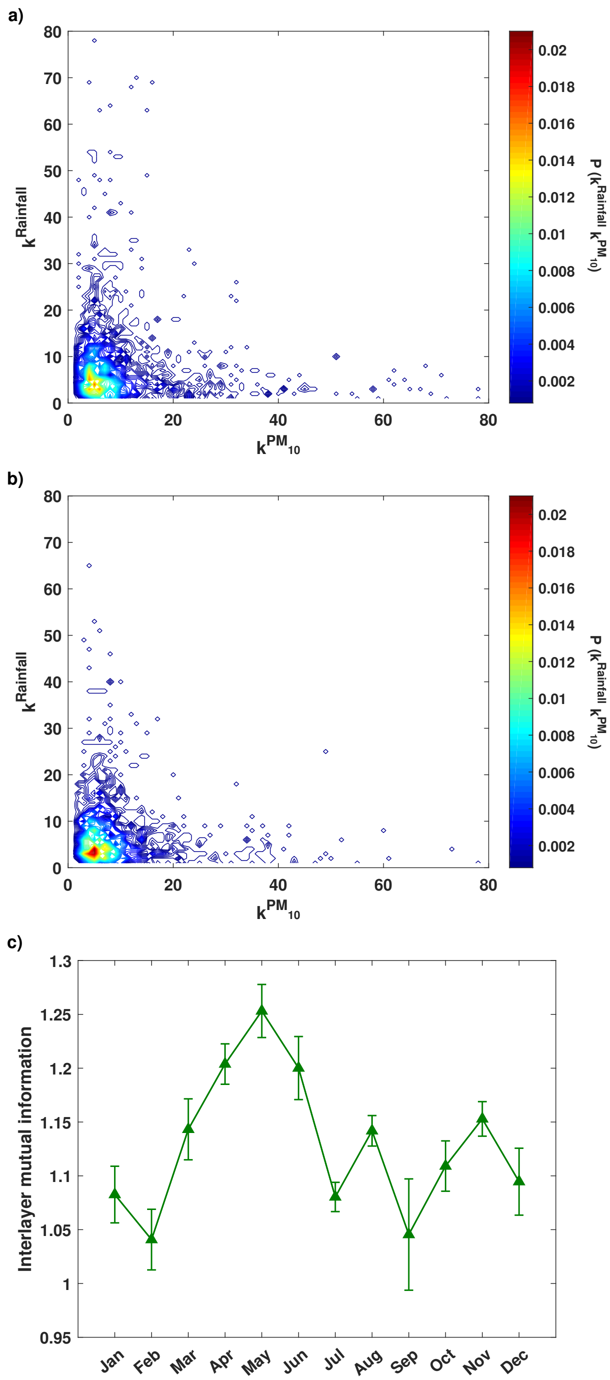

Figure 7: Illustration of the joint probability distribution of the degrees of both layers for (a) the low dust season (October to April) and (b) the high dust season (May to September) over an 11-y period. Each isoline shows the probability that the degree is precisely $k^{PM_{10}}$ and $k^{Rainfall}$ at the same time node in the VG frame; (c) monthly interlayer mutual information values ($I_{PM_{10}Rainfall}$) and their standard deviations computed over an 11-y period.

References

Adams, A.M., Prospero, J.M., Zhang, C.. CALIPSO-derived three-dimensional structure of aerosol over the Atlantic Basin and adjacent continents. Journal of Climate 2012;25(19):6862–6879.

Atkinson, R., Kang, S., Anderson, H., Mills, I., Walton, H.. Epidemiological time series studies of PM2.5 and daily mortality and hospital admissions: a systematic review and meta-analysis. Thorax 2014;69(7):660–665.

Battiston, F., Nicosia, V., Latora, V.. Structural measures for multiplex networks. Physical Review E 2014;89(3):032804.

Bayraktar, H., Turalioğlu, F.S., Tuncel, G.. Average mass concentrations of TSP, PM10 and PM2.5 in Erzurum urban atmosphere, Turkey. Stochastic Environmental Research and Risk Assessment 2010;24(1):57–65.

Bertin, A., Frangi, J.. Contribution to the study of the wind and solar radiation over guadeloupe. Energy Conversion and Management 2013;75:593–602.

Bianconi, G.. Statistical mechanics of multiplex networks: Entropy and overlap. Physical Review E 2013;87(6):062806.

Breslin, M., Belward, J.. Fractal dimensions for rainfall time series. Mathematics and computers in simulation 1999;48(4-6):437–446.

Carmona-Cabezas, R., Ariza-Villaverde, A.B., Gutiérrez de Ravé, E., Jiménez-Hornero, F.J.. Visibility graphs of ground-level ozone time series: A multifractal analysis. Science of The Total Environment 2019a;661:138–147.

Carmona-Cabezas, R., Gómez-Gómez, J., Ariza-Villaverde, A.B., Gutiérrez de Ravé, E., Jiménez-Hornero, F.J.. Multiplex Visibility Graphs as a complementary tool for describing the relation between ground level O_3 and No_2. Atmospheric Pollution Research 2020;11(1):205–212.

Carmona-Cabezas, R., Gómez-Gómez, J., Gutiérrez de Ravé, E., Jiménez-Hornero, F.J.. A sliding window-based algorithm for faster transformation of time series into complex networks. Chaos: An Interdisciplinary Journal of Nonlinear Science 2019b;29(10):103121.

Clergue, C., Dellinger, M., Buss, H., Gaillardet, J., Benedetti, M., Dessert, C.. Influence of atmospheric deposits and secondary minerals on Li isotopes budget in a highly weathered catchment, Guadeloupe (Lesser Antilles). Chemical Geology 2015;414:28–41.

Dallarosa, J.B., Teixeira, E.C., Pires, M., Fachel, J.. Study of the profile of polycyclic aromatic hydrocarbons in atmospheric particles (PM10) using multivariate methods. Atmospheric Environment 2005;39(35):6587–6596.

Van der Does, M., Brummer, G.J.A., van Crimpen, F.C., Korte, L.F., Mahowald, N.M., Merkel, U., Yu, H., Zuidema, P., Stuut, J.B.W.. Tropical rains controlling deposition of Saharan dust across the North Atlantic Ocean. Geophysical Research Letters 2020;47(5):e2019GL086867.

Dominguez, C., Done, J.M., Bruyère, C.L.. Easterly wave contributions to seasonal rainfall over the tropical Americas in observations and a regional climate model. Climate Dynamics 2020;54(1-2):191–209.

Dong, Q., Wang, Y., Li, P.. Multifractal behavior of an air pollutant time series and the relevance to the predictability. Environmental Pollution 2017;222:444–457.

Dunion, J.P.. Rewriting the climatology of the tropical North Atlantic and Caribbean Sea atmosphere. Journal of Climate 2011;24(3):893–908.

Engelstaedter, S., Tegen, I., Washington, R.. North African dust emissions and transport. Earth-Science Reviews 2006;79(1-2):73–100.

Euphrasie-Clotilde, L., Plocoste, T., Brute, F.N.. Particle Size Analysis of African Dust Haze over the Last 20 Years: A Focus on the Extreme Event of June 2020. Atmosphere 2021;12(4):502.

Euphrasie-Clotilde, L., Plocoste, T., Feuillard, T., Velasco-Merino, C., Mateos, D., Toledano, C., Brute, F.N., Bassette, C., Gobinddass, M.. Assessment of a new detection threshold for PM10 concentrations linked to African dust events in the Caribbean Basin. Atmospheric Environment 2020;224:117354.

Feng, W., Li, H., Wang, S., Van Halm-Lutterodt, N., An, J., Liu, Y., Liu, M., Wang, X., Guo, X.. Short-term PM10 and emergency department admissions for selective cardiovascular and respiratory diseases in Beijing, China. Science of The Total Environment 2019;657:213–221.

Giannini, A., Kushnir, Y., Cane, M.A.. Interannual variability of Caribbean rainfall, ENSO, and the Atlantic Ocean. Journal of Climate 2000;13(2):297–311.

González, C., Aristizábal, B.. Acid rain and particulate matter dynamics in a mid-sized Andean city: The effect of rain intensity on ion scavenging. Atmospheric Environment 2012;60:164–171.

Gouirand, I., Moron, V., Sing, B.. Seasonal atmospheric transitions in the Caribbean basin and Central America. Climate Dynamics 2020;55(7):1809–1828.

Gurung, A., Son, J.Y., Bell, M.L.. Particulate matter and risk of hospital admission in the Kathmandu Valley, Nepal: a case-crossover study. American journal of epidemiology 2017;186(5):573–580.

Iacovacci, J., Lacasa, L.. Visibility graphs for image processing. IEEE transactions on pattern analysis and machine intelligence 2019;42(4):974–987.

Johnson, R.H., Ciesielski, P.E.. Rainfall and radiative heating rates from TOGA COARE atmospheric budgets. Journal of the atmospheric sciences 2000;57(10):1497–1514.

Kidd, C., Huffman, G.. Global precipitation measurement. Meteorological Applications 2011;18(3):334–353.

Kim, J.E., Han, Y.J., Kim, P.R., Holsen, T.M.. Factors influencing atmospheric wet deposition of trace elements in rural Korea. Atmospheric Research 2012;116:185–194.

Kivelä, M., Arenas, A., Barthelemy, M., Gleeson, J.P., Moreno, Y., Porter, M.A.. Multilayer networks. Journal of complex networks 2014;2(3):203–271.

Kumar, A., Abouchami, W., Galer, S., Garrison, V., Williams, E., Andreae, M.. A radiogenic isotope tracer study of transatlantic dust transport from Africa to the Caribbean. Atmospheric Environment 2014;82:130–143.

Lacasa, L., Luque, B., Ballesteros, F., Luque, J., Nuno, J.C.. From time series to complex networks: The visibility graph. Proceedings of the National Academy of Sciences 2008;105(13):4972–4975.

Lacasa, L., Luque, B., Luque, J., Nuno, J.C.. The visibility graph: A new method for estimating the Hurst exponent of fractional Brownian motion. EPL (Europhysics Letters) 2009;86(3):30001.

Lacasa, L., Nicosia, V., Latora, V.. Network structure of multivariate time series. Scientific reports 2015;5:15508.

Lacasa, L., Toral, R.. Description of stochastic and chaotic series using visibility graphs. Physical Review E 2010;82(3):036120.

Lan, X., Mo, H., Chen, S., Liu, Q., Deng, Y.. Fast transformation from time series to visibility graphs. Chaos: An Interdisciplinary Journal of Nonlinear Science 2015;25(8):083105.

Laouali, D., Galy-Lacaux, C., Diop, B., Delon, C., Orange, D., Lacaux, J., Akpo, A., Lavenu, F., Gardrat, E., Castera, P.. Long term monitoring of the chemical composition of precipitation and wet deposition fluxes over three Sahelian savannas. Atmospheric environment 2012;50:314–327.

Latora, V., Nicosia, V., Russo, G.. Complex networks: principles, methods and applications. Cambridge University Press, 2017.

Lu, F., Xu, D., Cheng, Y., Dong, S., Guo, C., Jiang, X., Zheng, X.. Systematic review and meta-analysis of the adverse health effects of ambient PM2.5 and PM10 pollution in the Chinese population. Environmental research 2015;136:196–204.

Luque, B., Lacasa, L., Ballesteros, F., Luque, J.. Horizontal visibility graphs: Exact results for random time series. Physical Review E 2009;80(4):046103.

Mali, P., Manna, S., Mukhopadhyay, A., Haldar, P., Singh, G.. Multifractal analysis of multiparticle emission data in the framework of visibility graph and sandbox algorithm. Physica A: Statistical Mechanics and its Applications 2018;493:253–266.

Maskey, M., Puente, C., Sivakumar, B., Cortis, A.. Encoding daily rainfall records via adaptations of the fractal multifractal method. Stochastic Environmental Research and Risk Assessment 2016;30(7):1917–1931.

McClintock, M., McDowell, W., González, G., Schulz, M., Pett-Ridge, J.. African dust deposition in Puerto Rico: Analysis of a 20-year rainfall chemistry record and comparison with models. Atmospheric Environment 2019;216:116907.

Momtazan, M., Geravandi, S., Rastegarimehr, B., Valipour, A., Ranjbarzadeh, A., Yari, A.R., Dobaradaran, S., Bostan, H., Farhadi, M., Darabi, F., Khaniabadi, Y.O., Mohammadi, M.J.. An investigation of particulate matter and relevant cardiovascular risks in Abadan and Khorramshahr in 2014–2016. Toxin reviews 2019;38(4):290–297.

Moulin, C., Lambert, C.E., Dulac, F., Dayan, U.. Control of atmospheric export of dust from North Africa by the North Atlantic Oscillation. Nature 1997;387(6634):691–694.

Muñoz, E., Busalacchi, A.J., Nigam, S., Ruiz-Barradas, A.. Winter and summer structure of the Caribbean low-level jet. Journal of Climate 2008;21(6):1260–1276.

Murakami, M., Kimura, T., Magono, C., Kikuchi, K.. Observations of precipitation scavenging for water-soluble particles. Journal of the Meteorological Society of Japan Ser II 1983;61(3):346–358.

Nicosia, V., Latora, V.. Measuring and modeling correlations in multiplex networks. Physical Review E 2015;92(3):032805.

Nikolopoulos, D., Moustris, K., Petraki, E., Koulougliotis, D., Cantzos, D.. Fractal and Long-Memory Traces in PM10 Time Series in Athens, Greece. Environments 2019;6(3):29.

Olsson, J., Niemczynowicz, J., Berndtsson, R.. Fractal analysis of high-resolution rainfall time series. Journal of Geophysical Research: Atmospheres 1993;98(D12):23265–23274.

Olszowski, T.. Comparison of PM10 washout on urban and rural areas. Ecological Chemistry and Engineering S 2017;24(3):381–395.

Ouyang, W., Guo, B., Cai, G., Li, Q., Han, S., Liu, B., Liu, X.. The washing effect of precipitation on particulate matter and the pollution dynamics of rainwater in downtown Beijing. Science of the Total Environment 2015;505:306–314.

Peel, M.C., Finlayson, B.L., McMahon, T.A.. Updated world map of the köppen-geiger climate classification. Hydrology and Earth System Sciences 2007;11:1633–1644.

Perry, K.D., Cahill, T.A., Eldred, R.A., Dutcher, D.D., Gill, T.E.. Long-range transport of North African dust to the eastern United States. Journal of Geophysical Research: Atmospheres 1997;102(D10):11225–11238.

Petit, R., Legrand, M., Jankowiak, I., Molinié, J., Asselin de Beauville, C., Marion, G., Mansot, J.. Transport of Saharan dust over the Caribbean Islands: Study of an event. Journal of Geophysical Research: Atmospheres 2005;110:D18S09.

Pierini, J.O., Lovallo, M., Telesca, L.. Visibility graph analysis of wind speed records measured in central argentina. Physica A: Statistical Mechanics and its Applications 2012;391(20):5041–5048.

Pillai, P.S., Babu, S.S., Moorthy, K.K.. A study of pm, pm10 and pm2.5 concentration at a tropical coastal station. Atmospheric Research 2002;61(2):149–167.

Plocoste, T., Calif, R.. Spectral Observations of PM10 Fluctuations in the Hilbert Space. In: Functional Calculus. IntechOpen; 2019. p. 1–13.

Plocoste, T., Calif, R., Euphrasie-Clotilde, L., Brute, F.N.. Investigation of local correlations between particulate matter (PM10) and air temperature in the Caribbean basin using Ensemble Empirical Mode Decomposition. Atmospheric Pollution Research 2020a;11(10):1692–1704.

Plocoste, T., Calif, R., Euphrasie-Clotilde, L., Brute, F.N.. The statistical behavior of PM10 events over guadeloupean archipelago: Stationarity, modelling and extreme events. Atmospheric Research 2020b;241:104956.

Plocoste, T., Calif, R., Jacoby-Koaly, S.. Temporal multiscaling characteristics of particulate matter $PM10$ and ground-level ozone O_3 concentrations in Caribbean region. Atmospheric Environment 2017;169:22–35.

Plocoste, T., Calif, R., Jacoby-Koaly, S.. Multi-scale time dependent correlation between synchronous measurements of ground-level ozone and meteorological parameters in the Caribbean Basin. Atmospheric Environment 2019;211:234–246.

Plocoste, T., Carmona-Cabezas, R., Jiménez-Hornero, F.J., Gutiérrez de Ravé, E.. Background PM10 atmosphere: In the seek of a multifractal characterization using complex networks. Journal of Aerosol Science 2021a;155:105777.

Plocoste, T., Carmona-Cabezas, R., Jiménez-Hornero, F.J., Gutiérrez de Ravé, E., Calif, R.. Multifractal characterisation of particulate matter (PM10) time series in the Caribbean basin using visibility graphs. Atmospheric Pollution Research 2021b;12(1):100–110.

Plocoste, T., Dorville, J.F., Monjoly, S., Jacoby-Koaly, S., André, M.. Assessment of Nitrogen Oxides and Ground-Level Ozone behavior in a dense air quality station network: Case study in the Lesser Antilles Arc. Journal of the Air & Waste Management Association 2018;68(12):1278–1300.

Plocoste, T., Jacoby-Koaly, S., Molinié, J., Petit, R.. Evidence of the effect of an urban heat island on air quality near a landfill. Urban Climate 2014;10:745–757.

Plocoste, T., Pavón-Domínguez, P.. Multifractal detrended cross-correlation analysis of wind speed and solar radiation. Chaos: An Interdisciplinary Journal of Nonlinear Science 2020a;30(11):113109.

Plocoste, T., Pavón-Domínguez, P.. Temporal scaling study of particulate matter (PM10) and solar radiation influences on air temperature in the Caribbean basin using a 3D joint multifractal analysis. Atmospheric Environment 2020b;222:117115.

Prospero, J.M.. Long-range transport of mineral dust in the global atmosphere: Impact of African dust on the environment of the southeastern United States. Proceedings of the National Academy of Sciences 1999;96(7):3396–3403.

Prospero, J.M., Carlson, T.N.. Saharan air outbreaks over the tropical North Atlantic. In: Weather and Weather Maps. Springer; 1981. p. 677–691.

Prospero, J.M., Collard, F.X., Molinié, J., Jeannot, A.. Characterizing the annual cycle of African dust transport to the Caribbean Basin and South America and its impact on the environment and air quality. Global Biogeochemical Cycles 2014;28:757–773.

Prospero, J.M., Lamb, P.J.. African droughts and dust transport to the Caribbean: Climate change implications. Science 2003;302(5647):1024–1027.

Rastelli, E., Corinaldesi, C., Dell'Anno, A., Martire, M.L., Greco, S., Facchini, M.C., Rinaldi, M., O'Dowd, C., Ceburnis, D., Danovaro, R.. Transfer of labile organic matter and microbes from the ocean surface to the marine aerosol: an experimental approach. Scientific reports 2017;7(1):11475.

Schneider, U., Becker, A., Finger, P., Meyer-Christoffer, A., Ziese, M., Rudolf, B.. GPCC's new land surface precipitation climatology based on quality-controlled in situ data and its role in quantifying the global water cycle. Theoretical and Applied Climatology 2014;115(1-2):15–40.

Schumann, T.. Large discrepancies between theoretical and field-determined scavenging coefficients. Journal of Aerosol Science 1989;20(8):1159–1162.

Singh, S., Elumalai, S.P., Pal, A.K.. Rain pH estimation based on the particulate matter pollutants and wet deposition study. Science of the total environment 2016;563:293–301.

Sonwani, S., Kulshrestha, U.C.. PM10 carbonaceous aerosols and their real-time wet scavenging during monsoon and non-monsoon seasons at Delhi, India. Journal of Atmospheric Chemistry 2019;76(3):171–200.

Tartaglione, C.A., Smith, S.R., O'Brien, J.J.. ENSO impact on hurricane landfall probabilities for the Caribbean. Journal of Climate 2003;16(17):2925–2931.

Tiwari, S., Chate, D., Pragya, P., Ali, K., Bisht, D.S.. Variations in mass of the PM10, PM2.5 and PM 1 during the monsoon and the winter at New Delhi. Aerosol and Air Quality Research 2012;12(1):20–29.

Tombette, M., Mallet, V., Sportisse, B.. PM10 data assimilation over Europe with the optimal interpolation method. Atmospheric Chemistry and Physics 2009;9:57–70.

Weinmayr, G., Romeo, E., De Sario, M., Weiland, S.K., Forastiere, F.. Short-term effects of PM10 and NO2 on respiratory health among children with asthma or asthma-like symptoms: a systematic review and meta-analysis. Environmental health perspectives 2010;118(4):449–457.

Winstanley, D.. Rainfall patterns and general atmospheric circulation. Nature 1973;245(5422):190–194.

Wu, Y., Liu, J., Zhai, J., Cong, L., Wang, Y., Ma, W., Zhang, Z., Li, C.. Comparison of dry and wet deposition of particulate matter in near-surface waters during summer. PloS one 2018;13(6):e0199241.

Yoo, J.M., Lee, Y.R., Kim, D., Jeong, M.J., Stockwell, W.R., Kundu, P.K., Oh, S.M., Shin, D.B., Lee, S.J.. New indices for wet scavenging of air pollutants (O3, CO, NO2, SO2, and PM10) by summertime rain. Atmospheric Environment 2014;82:226–237.

Zhang, J., Liu, Y., Cui, L.l., Liu, S.q., Yin, X.x., Li, H.c.. Ambient air pollution, smog episodes and mortality in Jinan, China. Scientific reports 2017;7(1):1–8.

Declaration of interests

☒ The authors declare that they have no known competing financial interests or personal relationships that could have appeared to influence the work reported in this paper.

☐The authors declare the following financial interests/personal relationships which may be considered as potential competing interests:

Credit author statement

Thomas Plocoste: Conceptualization, Methodology, Software, Resources, Formal analysis, Data Curation, Visualization, Validation, Investigation, Project administration, Writing - original draft, Writing – review & editing**.**

Rafael Carmona-Cabezas: Methodology, Visualization, Formal analysis, Supervision, Validation, Investigation, Writing - original draft, Writing - review & editing**.**

Eduardo Gutiérrez de Ravé: Supervision, Writing – review & editing**.**

Francisco José Jiménez-Hornero: Supervision, Writing – review & editing**.**

Highlights

Multiplex visibility graphs as a useful tool for PM_{10} wet scavenging investigation

PM_{10} and rainfall hubs linked to their highest values in visibility graph frame

Significant annual variation in wet deposition efficiency

Identification of winter-summer transition periods

Graphical Abstract